Journal of Alloys and Compounds 480 (2009) 670–673

Contents lists available at ScienceDirect

Journal of Alloys and Compounds

journal homepage: www.elsevier.com/locate/jallcom

Microstructure and magnetic properties of $(Nd_{1-y}Pr_y)_{4.5}Fe_{77}B_{18.5}$ nanocomposite alloys

M. Rajasekhar [a,b], D. Akhtar [a,*], V. Chandrasekaran [a], S. Ram [b]

[a] Defence Metallurgical Research Laboratory, Hyderabad 500 058, India
[b] Materials Science Centre, Indian Institute of Technology, Kharagpur 721 302, India

ARTICLE INFO

Article history:
Received 25 December 2008
Received in revised form 25 January 2009
Accepted 31 January 2009
Available online 10 February 2009

Keywords:
Permanent magnets
$Fe_3B/Nd_2Fe_{14}B$ nanocomposite
Exchange coupling

ABSTRACT

Microstructure and magnetic properties of melt-spun $Fe_3B/Nd_2Fe_{14}B$ nanocomposites with compositions $(Nd_{1-y}Pr_y)_{4.5}Fe_{77}B_{18.5}$ (y = 0.00, 0.22, 0.45 and 0.66) have been investigated. Pr addition improves coercivity ($_iH_c$) and energy product $(BH)_{max}$ significantly from 2.6 kOe and 9.1 MGOe for y = 0.00 to 3.6 kOe and 13.2 MGOe for y = 0.45, but decreases remanent magnetization (M_r). Further increase in Pr weakens the exchange coupling interactions between the magnetically hard and soft phases. Effect of Pr on thermal stability of $_iH_c$ and M_r is analyzed by performing high temperature magnetic measurements. Thermal stability of $_iH_c$ decreases on Pr addition, whereas, that of M_r is not affected significantly. Microstructural parameters α and N_{eff} describing the influence of the non-ideal microstructure and the effect of exchange coupling on the coercivity are determined from the temperature dependence of coercivity.

1. Introduction

Nanocomposite magnets consisting of a fine mixture of hard-magnetic $Nd_2Fe_{14}B$ and soft-magnetic Fe_3B/α-Fe phases with grain size in nanometer scale are potential materials for permanent magnet applications [1–5]. They exhibit remanent magnetization (M_r) exceeding Stoner–Wohlfarth limit of $0.5M_s$, where M_s is saturation magnetization [1]. This behavior, known as enhanced remanence, is associated with exchange coupling interactions between the hard and soft magnetic grains. Depending on the volume fractions of the soft and hard magnetic phases the coercivity ($_iH_c$) adopts a value between 2 and 4 kOe [1,6]. A disadvantage of the nanocomposite alloys is the decrease in $_iH_c$ accompanying the M_r enhancement, which adversely affects $(BH)_{max}$, in spite of the continuing increase in M_r. Many attempts have been made to improve $_iH_c$ and $(BH)_{max}$ of the nanocomposites further by elemental substitution [7–11]. One such attempt is partial replacement of Nd by Pr or Dy rare earth elements. The magnetocrystalline anisotropy field (H_A) of $Pr_2Fe_{14}B$ phase is higher compared to that of $Nd_2Fe_{14}B$ [12]. There are several reports on Pr substitution for Nd showing an increase in $_iH_c$ in single phase $(Nd,Pr)_2Fe_{14}B$ as well as nanocomposite α-Fe/$(Nd,Pr)_2Fe_{14}B$ [13,14]. Barra-Barrera et al. studied the magnetic properties of $Fe_3B/Pr_2Fe_{14}B$ nanocomposite alloys [15]. In the present study we have carried out a systematic study of the effect of Pr substitution on the magnetic properties, their temperature dependence and exchange coupling behavior in melt-spun $Fe_3B/Nd_2Fe_{14}B$ nanocomposites with compositions $(Nd_{1-y}Pr_y)_{4.5}Fe_{77}B_{18.5}$ (y = 0.0, 0.22, 0.45 and 0.66).

2. Experimental

Alloy ingots with compositions $(Nd_{1-y}Pr_y)_{4.5}Fe_{77}B_{18.5}$ (y = 0.0, 0.22, 0.45 and 0.66) were prepared by vacuum arc-melting. The ingots were melted four times to ensure homogeneity. The arc-melted buttons were broken into small pieces and melt-spun in argon atmosphere using a quartz nozzle with an orifice diameter of ~1 mm. A wheel speed of 50 m/s was used to produce amorphous ribbons of the alloys. The ribbons obtained are ~3 mm wide and ~35 μm thick. The crystallization temperatures of the as-spun ribbons were determined using differential scanning calorimeter (TA instruments DSC-910) at a heating rate of 20 K/min under Ar gas flow. The as-spun ribbons were vacuum-sealed in quartz tubes and annealed at temperatures ranging from 863 to 988 K for 10 min to obtain fine nanosized grains and optimize the magnetic properties. Phase identification of the as-spun and annealed ribbons was carried out by X-ray diffraction (XRD) using a Philips PW-3020 diffractometer with 0.154056 nm Cu Kα radiation and thermomagnetic measurements. Microstructure studies were carried out using transmission electron microscope (TEM) (Technai F-20). Magnetic properties of the as-spun and annealed ribbons were measured using a vibrating sample magnetometer (DMS model ADE-EV9) with a maximum applied field of 20 kOe along the ribbon length. Magnetic phases present in the heat-treated ribbons and their Curie temperatures (T_C) were determined from thermomagnetic curves measured at a bias field of 1 kOe. The temperature dependence of M_r and $_iH_c$ was characterized by determining the temperature coefficients $\alpha(Mr)$ and $\beta(_iH_c)$, where:

$$\alpha(M_r) = \frac{[M_r(T_1) - M_r(T_2)]}{M_r(T_1)[T_1 - T_2]}, \quad (1)$$

$$\beta(_iH_c) = \frac{[_iH_c(T_1) - {}_iH_c(T_2)]}{_iH_c(T_1)[T_1 - T_2]}. \quad (2)$$

* Corresponding author. Fax: +91 40 24340884.
E-mail addresses: akhtaramg@yahoo.co.in, raj81hi@yahoo.com (D. Akhtar).

0925-8388/$ – see front matter © 2009 Elsevier B.V. All rights reserved.
doi:10.1016/j.jallcom.2009.01.125

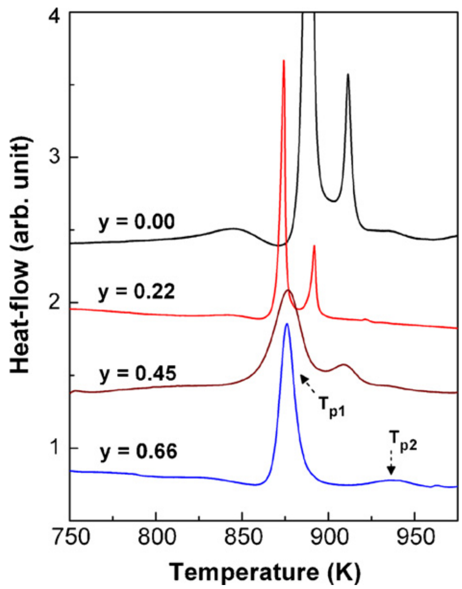

Fig. 1. DSC thermograms of melt-spun $(Nd_{1-y}Pr_y)_{4.5}Fe_{77}B_{18.5}$ (y = 0.00, 0.22, 0.45 and 0.66) alloys at a heating rate of 20 K/min.

3. Results and discussion

From XRD studies, all the as-spun ribbons are found to be amorphous. Fig. 1 shows the DSC plots of as-spun $(Nd_{1-y}Pr_y)_{4.5}Fe_{77}B_{18.5}$ (y = 0.00, 0.22, 0.45 and 0.66) ribbons. All the thermograms show two exothermic peaks with peak temperatures T_{p1} and T_{p2}. With addition of Pr, the peak T_{p1} shifts slightly toward lower temperature side, and the peak T_{p2} shifts toward higher temperature side. Fig. 2 shows the typical XRD patterns of y = 0.45 ribbons, both as-spun and annealed at 898 K (after T_{p1}) and 978 K (after T_{p2}). From XRD studies it is evident that the desired $(Nd,Pr)_2Fe_{14}B$ and Fe_3B composite crystallizes out of amorphous phase in two stages. The metastable $(Nd,Pr)_2Fe_{23}B_3$ phase, which crystallizes along with Fe_3B phase in the first stage (T_{p1}), decomposes to form $(Nd,Pr)_2Fe_{14}B$ and Fe_3B during the second stage (T_{p2}) [11,16,17]. Similar crystallization behavior has been observed for all the other ribbons also. Fig. 3 shows the typical TEM micrographs of y = 0.45 optimally annealed ribbon. The average grain size is estimated to be ~40 nm for all the optimally annealed ribbons. Thermomagnetic curves of optimally annealed $(Nd_{1-y}Pr_y)_{4.5}Fe_{77}B_{18.5}$ (y = 0.0, 0.22, 0.45 and 0.66) ribbons showing two magnetic transitions are presented in Fig. 4. The first transition corresponds to the T_C of $(Nd,Pr)_2Fe_{14}B$ phase and the second transition is due to the T_C of Fe_3B phase. T_C of $(Nd,Pr)_2Fe_{14}B$ phase decreases slightly on Pr addition, whereas the T_C of Fe_3B remains unchanged.

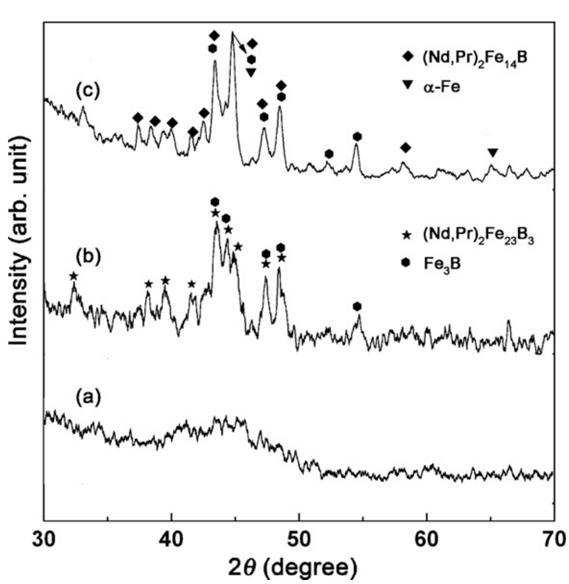

Fig. 2. Typical XRD patterns of $(Nd_{1-y}Pr_y)_{4.5}Fe_{77}B_{18.5}$ (y = 0.45) ribbons: (a) as spun, (b) annealed at 898 K, and (c) annealed at 978 K.

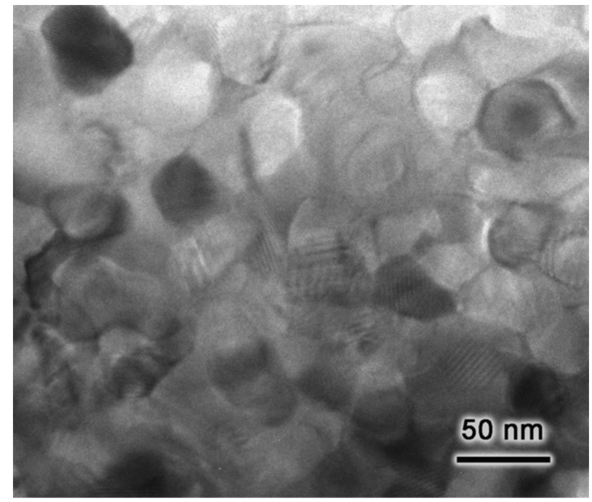

Fig. 3. TEM micrograph of $(Nd_{1-y}Pr_y)_{4.5}Fe_{77}B_{18.5}$ (y = 0.45) optimally annealed ribbon.

As-spun ribbons exhibit very low coercivity ($_iH_c$ <10 Oe). Annealing the as-spun ribbons at different temperatures, $_iH_c$ increases due to crystallization of the amorphous phase. The annealing temperatures to obtain optimum magnetic properties are

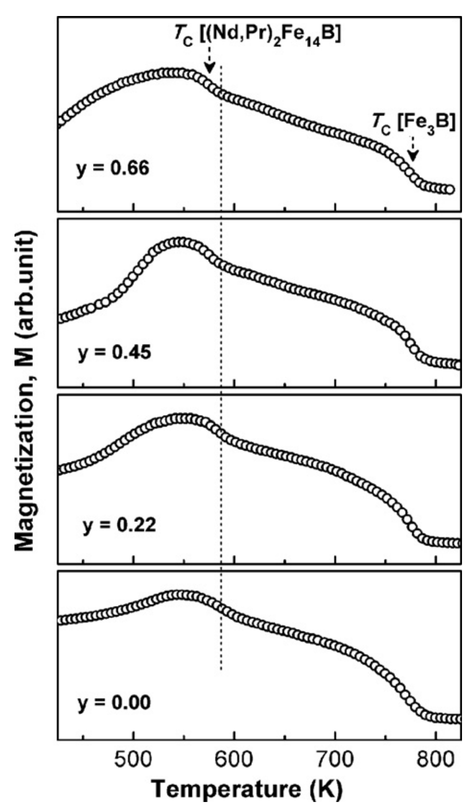

Fig. 4. Thermomagnetic curves of $(Nd_{1-y}Pr_y)_{4.5}Fe_{77}B_{18.5}$ (y = 0.00, 0.22, 0.45 and 0.66) optimally annealed ribbons.

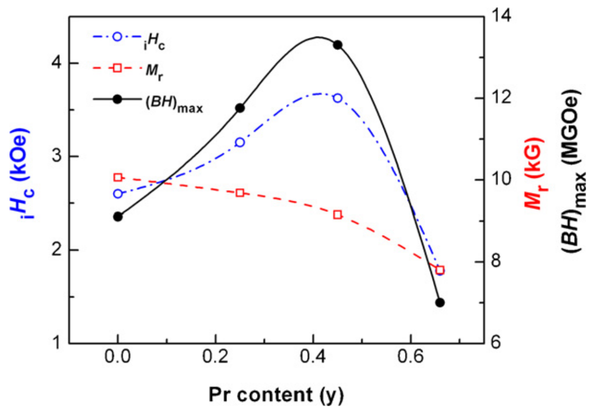

Fig. 5. Dependence of $_iH_c$, M_r and $(BH)_{max}$ on Pr content in $(Nd_{1-y}Pr_y)_{4.5}Fe_{77}B_{18.5}$ (y = 0.00, 0.22, 0.45 and 0.66) optimally annealed ribbons.

found to be 968 K for y = 0.00, 0.22 ribbons and 978 K for y = 0.45, 0.66 ribbons. Fig. 5 shows dependence of $_iH_c$, M_r and $(BH)_{max}$ on Pr content in optimally annealed ribbons. $_iH_c$ increases with increase in Pr content from 2.6 kOe at y = 0.00 and reaches a maximum value of 3.6 kOe at y = 0.45. Further increase in Pr content to y = 0.66 decreases the $_iH_c$ value to 1.8 kOe. M_r decreases continuously from 10.1 to 7.8 kG on increase in Pr from y = 0.00 to y = 0.66. However, $(BH)_{max}$ increases from 9.1 to 13.2 MGOe with increase in Pr from y = 0.0 to 0.45, and decreases with further increase in Pr as the $_iH_c$ and M_r values decreases. Increase in $_iH_c$ with increase in Pr up to y = 0.45 is due to increase in magnetocrystalline anisotropy field. Decrease in $_iH_c$ with further increase in Pr ($y > 0.45$) can be explained based on the model proposed by Kneller and Hawig [2]. The exchange coupling length in (b_{cm}) in nanocomposite system is expressed as:

$$b_{cm} = \pi\left(\frac{A_m}{2K_k}\right)^{1/2} \quad (3)$$

where, A_m is exchange energy of the soft phase and K_k is the magnetocrystalline anisotropy constant of the hard phase. To obtain sufficiently strong exchange coupling, the optimum grain size (b_m) of the soft phase should be approximately equal to b_{cm}. Substitution of Pr increases K_k of the hard magnetic phase [18] resulting in decrease of b_{cm} and particularly for y = 0.66 alloy the exchange coupling length becomes much lower to b_m resulting in incompletely coupled system. When a reverse field is applied, the moments of the soft phase decoupled from the hard phase, reverse at relatively small reverse field, which in turn make the hard phase moments to reverse resulting in very low $_iH_c$ value. The hysteresis loop looks uniform without showing any indication of two phases with extremely different coercivities. Xio et al. [19] and Yang et al. [20] exploited the effect of K_k on exchange length. They reported an increase in b_{cm} on Sm addition in $Nd_2Fe_{14}B/Fe_3B$ and $Nd_2Fe_{14}B/\alpha$-Fe systems. $Sm_2Fe_{14}B$ phase has negative value of K_k compared to $Nd_2Fe_{14}B$ phase and substitution of Sm to Nd decreases the K_k value of the hard $(Nd,Sm)_2Fe_{14}B$ phase resulting in increased b_{cm} following the Eq. (3).

Thermal stability of M_r and $_iH_c$ in optimally annealed $(Nd_{1-y}Pr_y)_{4.5}Fe_{77}B_{18.5}$ (y = 0.00, 0.22, 0.45) ribbons is evaluated by calculating temperature coefficients $\alpha(M_r)$ and $\beta(_iH_c)$ from hysteresis loops measured at different temperature in 273–523 K temperature range. Pr dependence of temperature coefficients α and β calculated using Eq. (1) and (2) are listed in Table 1. The value of α does not show much dependence, whereas the absolute value of β increases slightly from 0.323%/K to 0.349%/K on addition of Pr from y = 0.00 to y = 0.45. The increased temperature dependence of $_iH_c$ with Pr addition is consistent with the stronger temperature dependence of H_A in $Pr_2Fe_{14}B$ compared $Nd_2Fe_{14}B$ [12].

Table 1
Temperature of coefficients of $_iH_c$ and M_r for $(Nd_{1-y}Pr_y)_{4.5}Fe_{77}B_{18.5}$ (y = 0.00, 0.22, 0.45) optimally annealed ribbons.

y	Temperature coefficients (%/K)	
	$\alpha(M_r)$	$\beta(_iH_c)$
0.00	0.098	0.323
0.22	0.099	0.332
0.45	0.102	0.349

The coercivity in nanocrystalline two-phase magnet strongly depends on a broad set of crystallochemical and morphological features which influence the interaction between grains. The relationship between the microstructure and coercive in nanocrystalline magnets can be described by a modified form of Brown's equation [21–23]:

$$\frac{_iH_c(T)}{M_s(T)} = \alpha\frac{H_N^{min}(T)}{M_s(T)} - N_{eff} \quad (4)$$

where the microstructural parameters α and N_{eff} are related to the non-ideal microstructure of a realistic magnet. The microstructural parameter α takes into account the reduced surface anisotropy of nonperfect grains and as well describes the effect of exchange coupling between neighboring grains on the coercive field, and N_{eff} is an effective demagnetization factor describing the internal stray fields acting on the grains. H_N^{min} is the minimum nucleation field. From hysteresis loops measured at different temperatures the microstructural parameters α and N_{eff} are determined by plotting $_iH_c(T)M_s(T)$ vs. $H_N^{min}(T)/M_s(T)$. Fig. 6 shows $_iH_c(T)M_s(T)$ vs. $H_N^{min}(T)/M_s(T)$ plots corresponding to y = 0.00, 0.22 and 0.45 optimally annealed ribbons along with α and N_{eff} values. The best linear fit indicates that H_c is controlled by the nucleation process [22]. With increase in Pr content from y = 0.00 to y = 0.45, α value varies from 0.091 to 0.112. This increase in α can be attributed to decrease in the grain boundary defects with Pr addition [24]. N_{eff} values are estimated to be 0.042, 0.044 and 0.044. The extremely lower values of N_{eff} in the case of nanocomposite magnets indicate more spherical grain shape compared to conventional uncoupled melt-spun and sintered magnets.

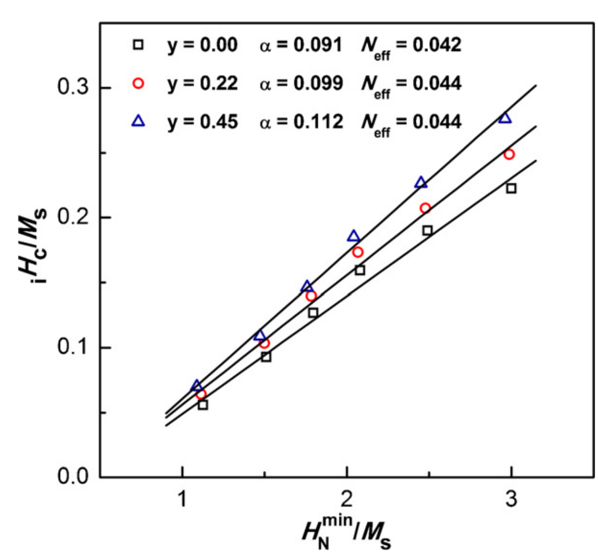

Fig. 6. $H_c(T)/M_s(T)$ vs. $H_N^{min}(T)/M_s(T)$ plots to determine the microstructural parameters α and N_{eff}.

4. Conclusions

Substitution of Pr for Nd improves ${}_iH_c$ and $(BH)_{max}$ of $Nd_{4.5}Fe_{77}B_{18.5}$ alloys, and optimum magnetic properties of ${}_iH_c$ = 3.6 kOe and $(BH)_{max}$ = 13.2 MGOe are obtained for y = 0.45 optimally annealed ribbons. Pr addition decreases T_C of $(Nd,Pr)_2Fe_{14}B$ phase slightly, whereas T_C of Fe_3B remains unchanged. Thermal stability of ${}_iH_c$ decreases slightly on Pr addition, while that of M_r is not affected much. Microsturcture parameter α and N_{eff} are determined from temperature dependence of ${}_iH_c$ and Pr addition decreases grain boundary defects.

Acknowledgements

This work was supported by DRDO, Govt. of India. Thanks are due to Dr A.K. Singh and Dr K. Suresh for their help in XRD and TEM. The authors are grateful to the Director, DMRL Hyderabad, for encouragement and permission to publish this paper.

References

[1] R. Coehoorn, D.B. de Mooij, J.P.W.B. Duchateau, K.H.J. Buschow, J. Phys. (Paris) Colloq. C8 669 (1988).
[2] E.F. Kneller, R. Hawig, IEEE Trans. Magn. 27 (1991) 3588.
[3] R. Fischer, T. Leineweber, H. Kronmuller, Phys. Rev. B 57 (1998) 10723.
[4] W.Y. Zhang, M. Stoica, J. Eckert, P. Yu, J.Z. Jiang, Intermetallics 16 (2008) 341.
[5] I. Betancourt, H.A. Davies, Appl. Phys. Lett. 87 (2005) 162516.
[6] L. Withanawasam, G.C. Hadjipanayis, J. Appl. Phys. 76 (1994) 7065.
[7] J.Q. Xie, C.H. Wu, Y.C. Chiang, F.M. Yang, Phys. Rev. B 41 (1990) 7162.
[8] W.C. Chang, S.H. Wu, B.M. Ma, C.O. Bounds, S.Y. Yao, J. Appl. Phys. 83 (1998) 2147.
[9] D.H. Ping, K. Hono, H. Kanekiyo, S. Hirosawa, Acta. Mater. 47 (4) (1999) 641.
[10] Z. Liu, H.A. Davies, J. Magn. Magn. Mater. 290 (2005) 1230.
[11] M. Rajasekhar, D. Akhtar, M.M. Raja, S. Ram, J. Magn. Magn. Mater. 320 (2008) 1645.
[12] S. Hirosawa, Y. Matsuura, H. Yamamoto, S. Fujimura, M. Sagawa, H. Yamauchi, J. Appl. Phys. 59 (1986) 873.
[13] J.I. Betancourt, R.H.A. Davies, J. Appl. Phys. 85 (1999) 5911.
[14] W. Zhang, S. Zhang, A. Yan, H. Zhang, B. Shen, J. Magn. Magn. Mater. 225 (2001) 389.
[15] A.D. Barra-Barrera, A.M. Pizzo, V. Villas-Boas, J. Magn. Magn. Mater. 302 (2006) 68.
[16] S. Nasu, T. Hinomura, S. Hirosawa, H. Kanekiyo, Physica B 237 (1997) 283.
[17] S. Hirosawa, H. Kanekiyo, Y. Shimemoto, K. Murakami, T. Miyoshi, Y. Shioya, J. Magn. Magn. Mater. 239 (2002) 424.
[18] Y.B. Kim, M.J. Kim, J. Han, T.K. Kim, J. Magn. Magn. Mater. 191 (1999) 133.
[19] Q.F. Xiao, T. Zhao, Z.D. Zhang, E. Brück, K.H.J. Bushow, F.R. de Boer, J. Magn. Magn. Mater. 223 (2001) 215.
[20] S. Yang, X. Song, B. Gu, Y. Du, J. Alloys Compd. 394 (2005) 1.
[21] M. Seeger, D. Köhler, H. Kronmüller, J. Magn. Magn. Mater. 130 (1994) 165.
[22] J. Bauer, M. Seeger, A. Zern, H. Kronmüller, J. Appl. Phys. 80 (1996) 1667.
[23] M. Rajasekhar, D. Akhtar, S. Ram, AIP Conf. Proc. 1003 (2008) 52.
[24] M. Seeger, D. Kohler, H. Kronmüller, J. Magn. Magn. Mater. 130 (1994) 165.